A simulation method for the calculation of chemical potentials in small, inhomogeneous, and dense systems

Alexander V. Neimark[a] and Aleksey Vishnyakov
Center for Modeling and Characterization of Nanoporous Materials, Textile Research Institute (TRI)/Princeton, Princeton, New Jersey 08542

(Received 1 March 2005; accepted 20 April 2005; published online 22 June 2005)

We present a modification of the gauge cell Monte Carlo simulation method [A. V. Neimark and A. Vishnyakov, Phys. Rev. E **62**, 4611 (2000)] designed for chemical potential calculations in small confined inhomogeneous systems. To measure the chemical potential, the system under study is set in chemical equilibrium with the gauge cell, which represents a finite volume reservoir of ideal particles. The system and the gauge cell are immersed into the thermal bath of a given temperature. The size of the gauge cell controls the level of density fluctuations in the system. The chemical potential is rigorously calculated from the equilibrium distribution of particles between the system cell and the gauge cell and does not depend on the gauge cell size. This scheme, which we call a mesoscopic canonical ensemble, bridges the gap between the canonical and the grand canonical ensembles, which are known to be inconsistent for small systems. The ideal gas gauge cell method is illustrated with Monte Carlo simulations of Lennard-Jones fluid confined to spherical pores of different sizes. Special attention is paid to the case of extreme confinement of several molecular diameters in cross section where the inconsistency between the canonical ensemble and the grand canonical ensemble is most pronounced. For sufficiently large systems, the chemical potential can be reliably determined from the mean density in the gauge cell as it was implied in the original gauge cell method. The method is applied to study the transition from supercritical adsorption to subcritical capillary condensation, which is observed in nanoporous materials as the pore size increases. © *2005 American Institute of Physics*. [DOI: 10.1063/1.1931663]

I. INTRODUCTION

The calculation of the chemical potential is one of the central problems in molecular simulations of phase and chemical equilibria. Starting with the seminal work of Widom,[1] a variety of computationally efficient methods have been proposed in the literature for determining the chemical potential in simple and complex homogeneous systems. However, in the case of small and inhomogeneous systems with highly curved interfaces, such as clusters, bubbles, and nanoconfined fluids, the problem of reliable practical calculations of chemical potentials is still unresolved.[2,3] In this paper, we suggest an efficient Monte Carlo (MC) simulation method using a new computational scheme called the mesoscopic canonical ensemble.

The original test particle insertion method of Widom[1] within the Metropolis MC simulation scheme[4] constitutes the primary tool for calculating the chemical potential in homogeneous phases. The Widom method implies random insertions of a test particle in the system equilibrated in the canonical ensemble and calculations of the average energy of its interactions with the real particles in the system. While the application of the Widom method for moderately dense fluids is straightforward and efficient, its implementation for dense systems is hindered by a vanishingly small probability of insertion.[2,3] Different modifications of the Widom method have been proposed to increase the efficacy of insertions. Such methods include methods which involve both particle insertions and removals,[5–8] the bicanonical ensemble method,[9] the Rosenbluth configurational-bias insertion schemes[10,11] and the recoil-growth techniques,[12,13] specifically designed for chain molecules, multistage insertion techniques,[6,14,15] the method of expanded ensembles,[16–18] and the umbrella sampling techniques.[19,20] This list can be extended. A comprehensive review on this topic may be found in Refs. 2 and 21 and more recent works.[22–24] As related to inhomogeneous systems subjected to external potential fields, the variety of available techniques is limited. Widom[25] has extended his original method to inhomogeneous systems and shown than the chemical potential is constant throughout the system. Thus, the chemical potential can, in principle, be calculated in any part of the system by test particle insertion.[2] Although the Widom method has been verified for some inhomogeneous systems,[26–28] its practical realization even with billions of test particle insertions can still result in large uncertainties.[29]

A few years ago, we proposed the gauge cell MC simulation method[30] for computing the chemical potential and studying the phase equilibrium in fluids confined to nanoscale pores. It was used to compute the adsorption isotherms and the vapor–liquid equilibrium of Lennard-Jones (LJ) fluid in cylindrical pores.[30] Since then, the gauge cell method found various applications in studies of phase behavior in nanoscale systems, including adsorption and capillary con-

[a]Author to whom correspondence should be addressed. Electronic mail: aneimark@triprinceton.org

densation of LJ fluid on mesoporous molecular sieves with cylindrical[30–32] and ink-bottle pores,[33] water on carbons,[34,35] and *n*-alkenes in carbon nanotubes,[36] formation of liquid bridges/junctions in nanocapillaries,[37] bubble cavitation in stretched metastable liquid,[38] and nucleation of droplets.[39] The gauge cell method was shown to be consistent with the results of the standard grand canonical Monte Carlo (GCMC) simulation method[40] in computing the adsorption isotherms of different fluids, and with the Peterson–Gubbins method[41] in computing the vapor–liquid equilibrium (VLE) in nanopores.[42] It was extended to include the configurational bias to simulate the phase behavior of chain molecules.[36] The simulated adsorption isotherms provide an accurate prediction of the experimental reversible and hysteretic capillary condensation isotherms on mesoporous molecular sieves of MCM-41 and SBA-15 types, including the positions of equilibrium and spinodal capillary condensation transitions.[35,36]

The gauge cell method[30] was developed to measure the chemical potential μ of the system of N particles confined to a finite volume V at a given temperature T in the presence of an external potential. As a case study system, one can imagine adsorption of a one-component fluid characterized by an intermolecular, fluid–fluid potential $\Phi_{\mathrm{FF}}(\mathbf{r}^N)$ in a pore with solid walls which exert a solid–fluid potential $\Phi_{\mathrm{SF}}(\mathbf{r}^N)$. In the following discussion, we will use this adsorption terminology. The chemical potential of the pore fluid is measured by considering it in the chemical equilibrium with the fluid confined to a gauge cell of volume V_g. The gauge cell does not contain any external potential and represents a finite reservoir of particles. The equation of state on the gauge fluid, i.e., its chemical potential μ_g as a function of the number of molecules N_g in the gauge cell, $\mu_g(N_g)$, is assumed known. This way, the gauge cell serves as a meter of the chemical potential of the pore fluid. The simulation is performed, similarly to the pore-fluid Gibbs ensemble MC (GEMC) scheme,[43,44] in a system of two cells (the pore cell and the gauge cell) with the exchange of particles between the cell at isothermal conditions to provide the chemical equilibrium. The total number of particles N_Σ is kept constant. The pore volume V and the gauge cell volume V_g are fixed. That is, one deals with the canonical ensemble of N_Σ particles, which are distributed between the two mechanically isolated cells.

In the original gauge cell method,[30] we suggested to compute the mean number of particles $\overline{N}$ and $\overline{N}_g$ in the pore and the gauge cells, and to define the chemical potential of the pore fluid comprised of $\overline{N}$ particles equal to the chemical potential of the gauge fluid comprised of $\overline{N}_g$ particles,

$$\mu(\overline{N}) = \mu_g(\overline{N}_g). \tag{1}$$

At the thermodynamic level, the simulation scheme corresponds to the minimization of the total Helmholtz free energy in the system of two cells,

$$F_\Sigma(N_\Sigma, V_\Sigma, T) = F(N, V, T) + F_g(N_g, V_g, T) \Rightarrow \min, \tag{2}$$

at the conditions

$$N_\Sigma = N + N_g = \mathrm{const}, \quad V, V_g, T = \mathrm{const}, \tag{3}$$

where subscript "g" denotes the gauge cell, and subscript "Σ" denotes the total simulation system. This scheme, called below the mean density gauge cell (MDGC) method, seems straightforward and well founded, provided the cells are large enough. In this case, minimization implies the equality of the chemical potentials [Eq. (1)], defined through the corresponding derivatives,

$$\mu = (\partial F/\partial N)_{V,T} = \mu_g = (\partial F_g/\partial N_g)_{V_g,T}. \tag{4}$$

However, dealing with small systems and, especially with phase transformations in small systems, which are of our primary interest, one encounters several fundamental problems, which are addressed in this paper. First, in small systems in the presence of density fluctuations, the mean density does not necessarily equal the most probable density, which is determined by the condition of minimization of the total Helmholtz free energy [Eq. (2)]. Second, Eq. (4) implies that the Helmholtz free energy is a continuous differentiable function that requires a sufficiently large size of the system. Third, the results obtained in different statistical ensembles are not equivalent in small systems so that the interpretation of the simulation results requires a special attention.[45] Fourth, the conditions of stability are different in open and closed small systems: the states, which are metastable or labile, such as nuclei, in the grand canonical ensemble, are stable in the canonical ensemble and can be sampled in the gauge cell method provided the gauge cell volume is sufficiently small.[30] This option opens up an opportunity to study the pathways of phase transformations and nucleation phenomena.[37,38]

The rest of the paper is structured as follows. In Sec. II we derive the statistico-mechanical equations underlying the gauge cell simulation method and show that the chemical potential can be rigorously calculated from the equilibrium distribution of particles between the system cell and the gauge cell and does not depend on the gauge cell size. In Sec. III, we suggest the ideal-gas gauge cell (IGGC) method. It is based on what we call a mesoscopic canonical ensemble (MCE), in which the system of interest is considered at the isothermal conditions in chemical equilibrium with a finite-volume reservoir of ideal particles that serves as the gauge cell. In Secs. IV–VI, the IGGC method is illustrated on simulations of Lennard-Jones fluid in spherical pores of different diameters to show its specifics and advantages, as compared with the Widom and MDGC methods, in studies of phase equilibria and phase transitions in nanoscale systems.

II. STATISTICAL MECHANICS OF THE GAUGE CELL METHOD

The Helmholtz free energy, $F(N,V,T)$, of a system of N particles (fluid molecules) confined to the pore of volume V at a given temperature T is defined through the canonical partition function

$$Q(N,V,T) = \frac{1}{\Lambda^{3N}N!}\int d\mathbf{r}^N \exp(-\Phi(\mathbf{r}^N)/kT), \tag{5}$$

where the total potential energy $\Phi(\mathbf{r}^N)$ is the sum of the fluid–fluid potential $\Phi_{FF}(\mathbf{r}^N)$ and the solid–fluid potential $\Phi_{SF}(\mathbf{r}^N)$, as

$$F(N,V,T) = -kT\ln Q(N,V,T). \tag{6}$$

The canonical chemical potential is defined as the difference of the Helmholtz free energies of the systems with $N+1$ and N molecules,

$$\begin{aligned}\mu^{+}_{CE}(N) &= F(N+1,V,T) - F(N,V,T)\\ &= -kT\ln\left(\frac{Q(N+1,V,T)}{Q(N,V,T)}\right)\\ &= -kT\ln\left(\frac{V}{\Lambda^3(N+1)}\right)\\ &\quad -kT\ln\left(\frac{1}{V}\int d\mathbf{r}_{N+1}\langle\exp(-\Phi(r_{N+1},\mathbf{r}^N)/kT)\rangle_N\right),\end{aligned} \tag{7}$$

where $\Phi(\mathbf{r}_{N+1},\mathbf{r}^N)=\Phi_{FF}(\mathbf{r}_{N+1},\mathbf{r}^N)+\Phi_{SF}(\mathbf{r}_{N+1})$ accounts for interactions of the $(N+1)$th molecule located at $\mathbf{r}_{N+1}$ with the remaining N molecules as a function of their positions $\mathbf{r}^N$ and with the pore walls. $\langle\cdots\rangle_N$ denotes the canonical ensemble average over the positions of N molecules.

The chemical potential $\mu^{+}_{CE}(N)$ represents the work of insertion of an additional molecule into the pore containing N molecules. This definition is equivalent to the Widom insertion method for computing the chemical potential in the canonical ensemble Monte Carlo method (CEMC).[2] It is worth noting that in the original paper,[1] Widom introduced the chemical potential (thermodynamic activity) in the system of N molecules as the difference of the Helmholtz free energies of the systems with N and $N-1$ molecules. If N is large enough, the difference of these definitions does not matter and the chemical potential can be defined through the derivative $\mu=(\partial F/\partial N)_{V,T}$, as implied in Eq. (3). However, for a rigorous treatment of small systems even one molecule counts.

Equation (7) defines the chemical potential as a discrete function of N through the finite differences of the Helmholtz free energy. Provided the integration in (7) is carried out over the entire configuration space, $\mu^{+}_{CE}(N)$ is a singe-valued function of the number of molecules in the system, or loading N. The inverse function, loading versus chemical potential $N(\mu)$, represents the canonical ensemble isotherm, which determines the phase behavior of the confined fluid.

In the gauge cell method, we allow the fluid, confined to the pore cell of volume V, to exchange particles with the gauge cell of volume V_g, which plays a role of the reservoir of a limited capacity. Both cells are immersed in the thermal bath maintaining a given temperature T. The total number of particles N_Σ in the system of two cells is fixed. The probability to observe a configuration of N molecules in the pore cell and, respectively, $N_g=N_\Sigma-N$ molecules in the gauge cell is proportional to

$$P_N = P_{N_g} \propto \exp\left\{-\frac{1}{kT}[F(N,V,T)+F_g(N_g,V_g,T)]\right\} \tag{8}$$

and, correspondingly,

$$\begin{aligned}P_{N+1} &= P_{N_g-1}\\ &\propto \exp\left\{-\frac{1}{kT}[F(N+1,V,T)+F_g(N_g-1,V_g,T)]\right\}.\end{aligned} \tag{9}$$

Thus, the canonical chemical potential of the series of (N,V,T) states sampled in the gauge cell simulation at a given N_Σ is determined from the ratio of the sampling probabilities. Taking into account Eq. (7), we obtain

$$\begin{aligned}\frac{P_{N+1}}{P_N} &= \frac{P_{N_g-1}}{P_{N_g}}\\ &= \exp\left\{-\frac{1}{kT}[\mu_{CE}(N,V,T)-\mu_g(N_g-1,V_g,T)]\right\},\end{aligned} \tag{10}$$

and

$$\mu_{CE}(N,V,T) = \mu_g(N_g-1,V_g,T) + kT\ln(P_{N_g}/P_{N_g-1}). \tag{11}$$

Equation (11) constitutes the foundation for computing the canonical isotherm of the pore fluid in the form of $\mu_{CE}(N)$ from the histograms of the distribution of particles in the gauge cell. Since in the derivation of Eq. (11) no assumptions or approximations were made, the result does not depend either on the size of the gauge cell V_g or on the total number of particles N_Σ in a given simulation. To construct the canonical isotherm one has to perform the gauge cell simulations varying the total number of particles in the system and/or the size of the gauge cell. In so doing, from one simulation at given N_Σ and V_g, several points of the isotherm can be computed around the most probable loading $\hat{N}$ with precision of a single molecule, as exemplified below.

The most probable distribution, which corresponds to the minimum of the total Helmholtz free energy [Eq. (2)], is determined by the nonequalities

$$\mu_{CE}(\hat{N}-1) < \mu_g(\hat{N}_g), \quad \mu_g(\hat{N}_g-1) \leqslant \mu_{CE}(\hat{N}). \tag{12}$$

If the loading is sufficiently large, $\hat{N}\gg 1$, the nonequalities [Eq. (12)] are reduced to the conventional condition of the equality of the chemical potentials,

$$\mu_{CE}(\hat{N}) = \mu_g(\hat{N}_g). \tag{13}$$

Equation (13) holds with uncertainty of $\max\{\mu_{CE}(N)-\mu_{CE}(N-1), \mu_g(N_g)-\mu_g(N_g-1)\}$. Besides, at sufficiently large loadings, the distribution of particles around the most probable loading is symmetric, and in Eq. (13) the most probable number of particles $\hat{N}$ can be replaced by the average $\overline{N}$, as implied by Eq. (1) employed in the original gauge cell method.[30,32] In Sec. IV, we demonstrate that equality (1) holds with a reasonable accuracy when the system accommodates more than $\sim$30–40 particles (reasonable accuracy means that the level of errors due to the approximation does

not exceed the natural noise level of simulation results).

III. IDEAL-GAS GAUGE CELL METHOD

The equations derived above do not imply any restrictions on the gauge cell and on the interactions of particles within the gauge cell. In the original method,[30,32] we suggested that the particles transferred from the pore cell into the gauge cell do not change their identity and interact according to the same intermolecular potential. As implemented in,[30,32,36] the gauge fluid was the bulk vapor confined to a box with periodic boundary conditions applied. In studies of LJ fluids,[30,32] the average density in the gauge cell was related to the chemical potential via the Johnson–Zollweg–Gubbins (JZG) equation of state.[46] In studies of hydrocarbons, Jiang *et al.*[36] measured the chemical potential in the gauge cell by means of the Widom method.[1]

The most practical and theoretically sound choice is to consider the particles in the gauge cell as ideal. In this case, the chemical potential of i particles in the gauge cell equals

$$\mu_{\mathrm{IG}}(i) = -kT\ln\left(\frac{V_g}{\Lambda^3(i+1)}\right), \tag{14}$$

and Eq. (11) reduces to

$$\mu_{\mathrm{CE}}(N,V,T) = -kT\ln\left(\frac{V_g}{\Lambda^3 N_g}\right) + kT\ln(P_{N_g}/P_{N_g-1}). \tag{15}$$

Correspondingly, at sufficiently large N, Eq. (1) reduces to

$$\mu_{\mathrm{CE}}(\overline{N},V,T) = -kT\ln\left(\frac{V_g}{\Lambda^3(\overline{N}_g+1)}\right). \tag{16}$$

The computational scheme of the IGGC method corresponds to the mesoscopic canonical ensemble (MCE), which is intermediate between the canonical ensemble (CE) and the grand canonical ensemble (GCE). In GCE, the system under study is open for the exchange of particles with the unlimited reservoir of ideal particles, so that the fluctuations of N are unconstrained. In CE, the system is closed and N is constant. In MCE, the system under study (pore of volume V) is semiopen: it exchanges particles with the finite-volume reservoir of ideal particles (gauge cell of volume V_g). Thus, the system mass fluctuates and the level of fluctuations is controlled by the reservoir volume V_g. This is the key property of MCE. As V_g increases, MCE transforms into GCE. As V_g diminishes, MCE reduces to CE.

The simulation procedure in the IGGC method is as follows. Three types of MC moves are performed: particle displacement within the pore cell, particle insertion into the pore cell from the gauge cell, and particle removal from the pore cell to the gauge cell. The displacement step in the pore cell is identical to that in the canonical ensemble: the trial move is accepted with the probability

$$p_{\mathrm{dis}} = \min\{1, \exp(-\Delta E/kT)\}, \tag{17}$$

where $\Delta E = \Delta\Phi_{\mathrm{FF}}(\mathbf{r}^N) + \Delta\Phi_{\mathrm{SF}}(\mathbf{r}^N)$ is the change of the configuration energy. A trial insertion into the pore cell from the gauge cell is accepted with the probability

$$p_{\mathrm{ins}} = \min\{1, \exp[-\Delta E/kT - \ln(V_g(N+1)/VN_g)]\}, \tag{18}$$

and a trial removal from the pore cell into the gauge cell is accepted with the probability

$$p_{\mathrm{rem}} = \min\{1, \exp[-\Delta E/kT - \ln(V(N_{g+1})/V_g N)]\}. \tag{19}$$

Acceptance probabilities (17)–(19) provide the fulfillment of the MCE particle distribution between the pore and gauge cells,

$$P_N = P_{N_g} = \frac{V^{N_g}}{N_g!\Lambda^{N_g}}\exp[-F(N,V,T)/kT]. \tag{20}$$

One insertion and one removal steps were attempted per each trial displacement.

The code for GCMC/CEMC/IGGC/MDGC simulations, which was applied in this paper, and the manual to the program are available as Supplementary Information.[47]

IV. EXAMPLES OF MONTE CARLO SIMULATIONS: EXTREME CONFINEMENT

We performed the IGGC simulations of sorption of a LJ fluid in a series of spherical pores of different diameters, $D = (4, 6, 8, 10,$ and $15.8)\sigma$ (that corresponds to internal diameters $D_{\mathrm{in}} = D - \sigma_{\mathrm{SF}}$ ranging from 1.17 to 5.44 nm). The LJ parameters of the fluid ($\varepsilon/k = 101.5$ K, $\sigma = 0.3615$ nm, $r_{\mathrm{cutoff}} = 5\sigma$) correspond to the model nitrogen.[48] The solid wall was modeled as a uniform layer of "smeared-out" LJ atoms which produces the solid–fluid potential[49]

$$U_{\mathrm{SF}}^{(\mathrm{sph})}(r,R) = 2\pi\rho_s\varepsilon_{\mathrm{SF}}\sigma_{\mathrm{SF}}^2\left[\frac{2}{5}\sum_{i=0}^{9}\left(\frac{\sigma_{\mathrm{SF}}^{10}}{R^i r^{10-i}} + (-1)^i\frac{\sigma_{\mathrm{SF}}^{10}}{R^i(r-2R)^{10-i}}\right) - \sum_{i=0}^{9}\left(\frac{\sigma_{\mathrm{SF}}^{4}}{R^i r^{4-i}} + (-1)^i\frac{\sigma_{\mathrm{SF}}^{4}}{R^i(r-2R)^{4-i}}\right)\right]. \tag{21}$$

In Eq. (17), r is the radial coordinate of the fluid molecule reckoned from the pore center, R is the pore radius, ρ_s is the surface number density of the adsorption centers, and $\varepsilon_{\mathrm{SF}}$ and σ_{SF} are the effective LJ parameters of the intermolecular solid–fluid interaction. As the pore size increases, the potential in (21) reduces to the 10-4 potential from a plane of LJ centers. We employed the LJ parameters of the potential $\sigma_{\mathrm{SF}} = 0.3494$ nm and $\varepsilon_{\mathrm{SF}}/k = 53.22$ K and $\rho_s = 15.3$ nm^{-2}, which were found in Ref. 50 from the best fit of the calculated nitrogen adsorption isotherm on the flat surface to the experimental isotherm on nonporous silica.[51] The solid–fluid potentials in the pores of different diameters are shown in Fig. 1. The depth of the potential well at the pore wall increases with the wall curvature.

Figure 2 shows the results of simulations for the smallest pore of diameter $D = 4\sigma$ at $kT/\varepsilon = 0.5$. This pore can accommodate just one layer of molecules at its wall with one molecule in the center. We fitted a maximum of 15 molecules in this system. The total number of molecules in the system N_Σ was varied from 6 to 20. As N_Σ was varied, the gauge cell volume V_g was adjusted to have on average about five molecules in the gauge cell. The length of simulations was about

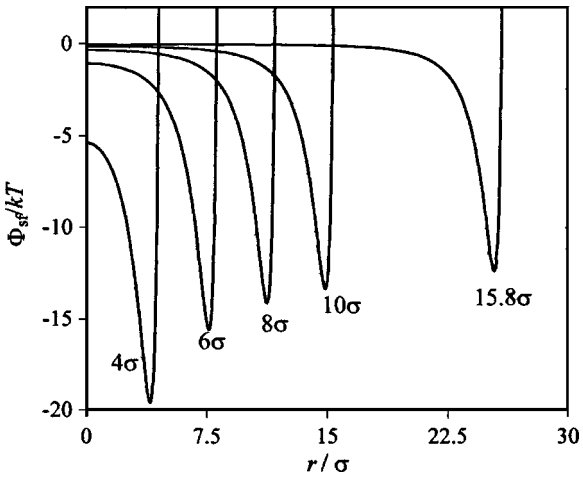

FIG. 1. Solid–fluid potentials in spherical pores of different diameters determined by Eq. (21) with the parameters mimicking adsorption of nitrogen on silica. r is the distance from the pore center.

5×10^5 steps per molecule. At each N_Σ, the histogram of the distribution of the number of particles in the gauge cell was computed, and the N_Σ points of the canonical isotherm $\mu_{CE}(N)$ were calculated according to Eq. (15). For example, at $N_\Sigma=11$, the histogram of N_g contains 12 columns [Fig. 2(a)], from which one can obtain 11 points of the canonical isotherm [open diamonds in Fig. 2(b)]. In Fig. 2(b), we present the overlapping results of simulations obtained at different N_Σ, which are in excellent agreement.

Note, that the leftmost point in Fig. 2(b) corresponds to the "empty cell" chemical potential $\mu^+_{CE}(0)$, defined as the work of insertion of the first molecule into the empty pore,

$$\mu^+_{CE}(0) = -kT\ln\left(\frac{V}{\Lambda^3}\right) - kT\ln\left(\frac{1}{V}\int \exp(-\Phi_{ext}(\mathbf{r})/kT)d\mathbf{r}\right) = -kT\ln\left(\frac{V_g}{\Lambda^3 N_g}\right) + kT\ln(P_{N_\Sigma}/P_{N_\Sigma-1}). \quad (22)$$

$\mu^+_{CE}(0)$ is determined by the pore volume V and solid–fluid potential $\Phi_{SF}(\mathbf{r}^N)$; the integral in Eq. (18) determines the Henry constant.[52] Equation (22) provides an additional validation of the correctness of the computational scheme.

In Fig. 2(b), we also present the results of the CE simulations with the chemical potential determined by the particle insertion method of Widom[1] in accordance with Eq. (7). At $N<12$, agreement between the gauge cell method and the Widom method is excellent. However, at high density, $N=12-14$, the Widom method deteriorates, and the simulation runs with up to 1×10^9 insertion attempts are insufficient for reliable estimates even in such a small pore. The quality of the Widom method improves as the temperature increases (see Fig. s1 in the Supplementary Information[47]) and declines rapidly as the system size increases.[47] It is worth noting that in all cases the statistical uncertainties of the IGGC method are substantially lower than those of the Widom method. We estimated that in the 4σ pore the gauge cell method converged about ten times faster than the Widom method.

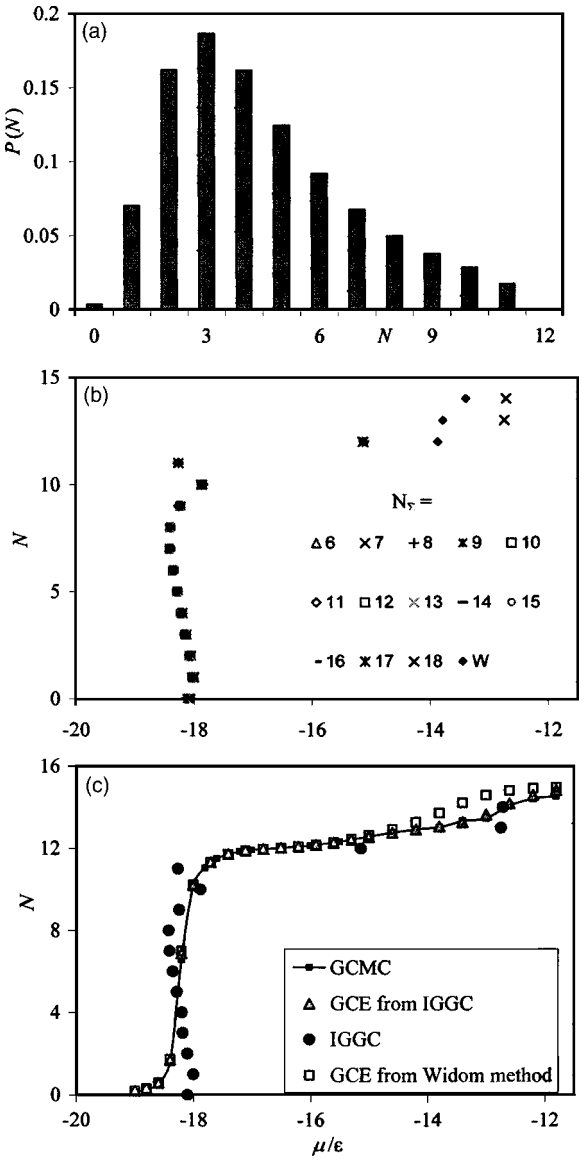

FIG. 2. Results of simulations in different ensembles in the 4σ pore at $kT/\varepsilon=0.5$. (a) IGGC method: Probability distribution of the number of molecules in the pore cell in MCE at $N_\Sigma=11$. (b) CE isotherms obtained in IGGC simulations with different N_Σ using Eq. (15). The gauge volume was changed to keep the average number of molecules in the gauge $\overline{N_\Sigma}\approx5$. Filled diamonds correspond to the isotherm determined in the CEMC simulation with the chemical potential determined with the Widom method; deviations are pronounced at high densities. (c) Comparison of CE and GCE isotherms: The CE isotherm (filled circles) was determined in the IGGC simulation. Three GCE isotherms were obtained in the direct GCMC simulation (curve) and recalculated using Eq. (24) from the CE isotherms determined in the IGGC simulation (triangles) and in CE simulation with the Widom method (squares).

The 4σ pore is a prominent example of small systems where the results obtained in different statistical ensembles deviate significantly. In Fig. 2(c), we present the CE isotherm (filled circles), constructed by averaging the overlapping points obtained in the IGGC simulation series with different N_Σ, and the GCE isotherm (solid line/small filled squares), generated in the standard GCMC simulation. The CE iso-

therm exhibits several distinct features that are not present on the GCE isotherm. The GCE isotherm is a monotonic single-valued function of μ, while the CE isotherm has a sigmoid shape at small N, an unexpected swing at $N=11$, and a step at $N=13$. Thus, the CE isotherm is more informative; it reflects the specifics of molecular packing, which are discussed below.

The GCE isotherm can be reconstructed from the CE isotherm that provides the additional test of the consistency of the simulations. The probability to observe N molecules in GCE at a given chemical potential μ is determined by the Helmholtz free energy F, which can be calculated from the CE isotherm as

$$F(N,V,T) = \sum_{i=0}^{N-1} \mu_{\mathrm{CE}}(i,V,T). \tag{23}$$

The loading computed in the GCMC method as a function of the chemical potential is the GCE average,

$$N_{\mathrm{GCE}}(\mu) = \sum_{N=0}^{\infty} N \exp(\mu N/kT - F(N,V,T)/kT)/\Xi(\mu,V,T), \tag{24}$$

where $\Xi(\mu,V,T)$ is the grand canonical partition function,

$$\Xi(\mu,V,T) = \sum_{N=0}^{\infty} \exp(\mu N/kT - F(N,V,T)/kT). \tag{25}$$

The GCE isotherm reconstructed from the CE isotherm obtained in the IGGC method [open triangles in Fig. 2(c)] excellently coincides with the GCMC isotherm. For comparison, we computed also the GCE isotherm reconstructed from the CE isotherm obtained with the Widom method [squares in Fig. 2(c)]. This isotherm agrees well with the GCMC simulation at $N<12$ and deviates appreciably at higher loadings thus confirming that the Widom method does not provide a required precision in high-density systems. We performed a similar analysis for higher temperatures up to $kT/\varepsilon=0.85$. The complete set of figures is given in the Supplementary Information,[47] We demonstrate that the results of the IGGC and GCMC simulations are consistent up to $N=16$.

The shape of the CE isotherm reflects the peculiarities of molecular packing and the stability of configurations at different loadings. For example, at $N=12$, the pore fluid exhibits a very symmetric fivefold configuration shown in Fig. 3(a). A prominent fivefold symmetry holds at $N=11$ [Fig. 3(b)] also. However, the fivefold symmetry is destroyed when another molecule is removed, as the configuration at $N=10$ is totally disordered. The histograms $P(N_g)$ at different N_Σ show clearly that the fivefold configuration at $N=11$ is preferential to $N=10$, which has a lower probability compared to the neighboring configurations [Fig. 3(d)].

V. EXAMPLES OF MONTE CARLO SIMULATIONS: INCREASING THE CONFINEMENT SIZE

In Figs. 4 and 5 we present the results of simulations of CE and GCE isotherms in pores of different diameters from

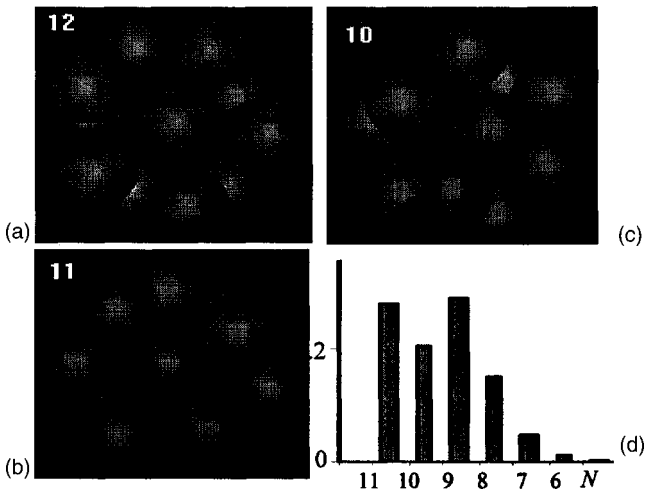

FIG. 3. Specifies of molecular packing in the 4σ pore: (a) a stable fivefold symmetry configuration at $N=12$, (b) a stable fivefold symmetry with a "vacancy" configuration at $N=11$, (c) a disordered configuration at $N=10$, and (d) a histogram of the number of molecules showing a minimum at $N=10$.

$D=4\sigma$ to $D=15.8\sigma$ at a higher temperature $kT/\varepsilon=0.762$. This temperature corresponds to the boiling temperature of model LJ nitrogen that allows one to compare the results of simulations with standard adsorption experiments. The capacity of confinements varied, respectively, from 16 to ~1500 molecules. The gauge cell size in these simulations was varied to keep $\overline{N_g}$ approximately constant: $\overline{N_g}\approx 5$ in 4σ and 6σ pores, $\overline{N_g}\approx 10$ in 8σ and 10σ pores, and $\overline{N_g}\approx 30$ in 15.8σ pore.

The CE isotherms demonstrate the transition from supercritical, monotonic isotherms in small pores (4σ and 6σ) to subcritical, van der Waals-type isotherms in larger pores (10σ and 15.8σ). 8σ is close to the critical pore size: the stepwise isotherm in the 8σ pore separates supercritical and subcritical CE isotherms in smaller and larger pores, respectively. Note that we consider here criticality in the canonical ensemble as the transition from singe-valued isotherms to multivalued isotherms with distinguishable low-density vaporlike and high-density liquidlike states characterized by the same chemical potential. The transition between these states is known as capillary condensation. Gauge cell method was first applied to capillary condensation criticality in cylindrical pores.[32]

One of our goals was to analyze the conditions of practical applicability of the MDGC method,[30,32] which is based on calculations of the chemical potential from the mean density in the gauge cell, as implied by Eqs. (1) and (16). An appreciable deviation of the IGGC and MDGC isotherms is observed in the smallest pore of 4σ and in the larger pores only at very low loadings less than ~10 molecules. Interestingly enough, the averaging over fluctuations results in almost indistinguishable isotherms obtained with the MDGC and GCMC methods in the 4σ pore. At larger loadings, the IGGC and MDGC isotherms agree within a reasonable accuracy; at $N>30$ they are practically indistinguishable. Thus, in pores larger 6σ the MDGC method can be safely applied to construct CE isotherms in both supercritical and subcritical regimes.

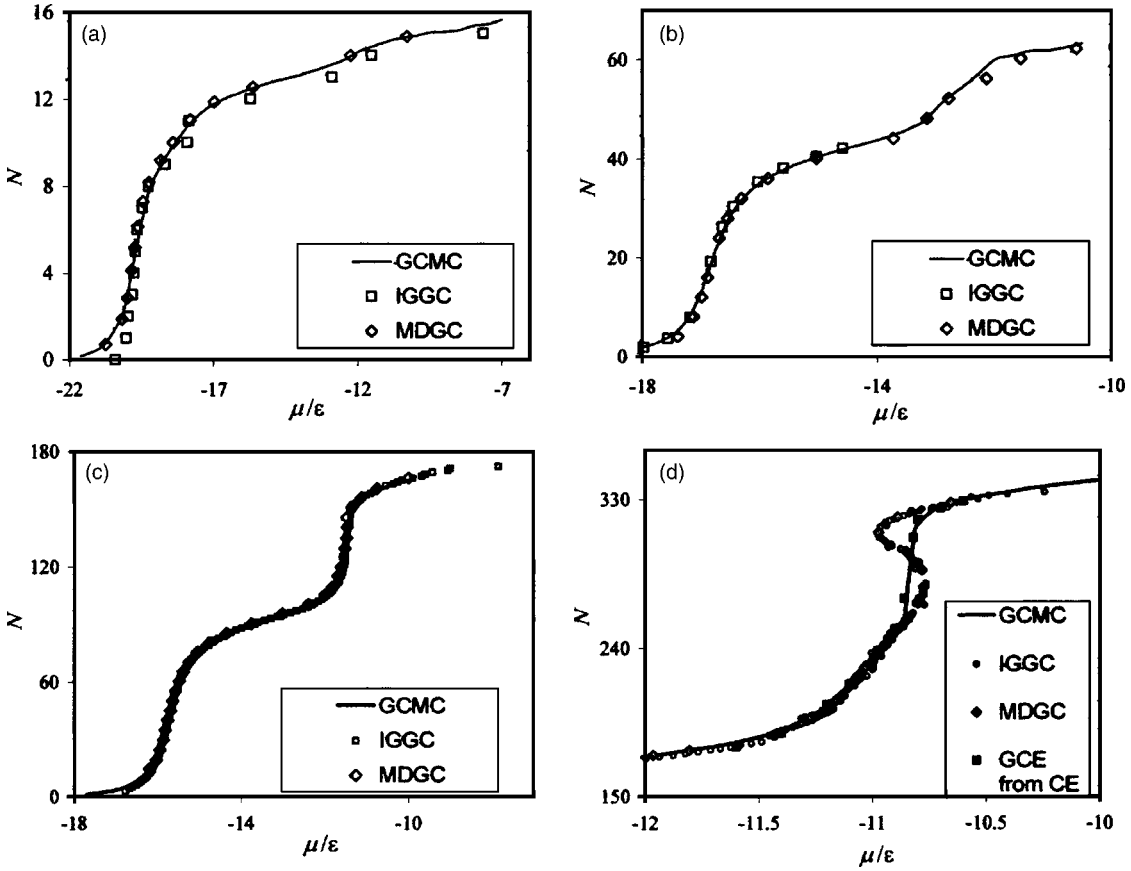

FIG. 4. Transition from supercritical adsorption to subcritical capillary condensation: comparison of the GCMC, IGGC, and MDGC methods in the pores of different diameters at $kT/\varepsilon=0.762$. (a) Supercritical adsorption in the 4σ pore: The MDGC isotherm substantially differs from the IGGC isotherm yet almost coincides with the GCMC isotherm. (b) Supercritical adsorption in the 6σ pore: The MDGC isotherm deviates from the IGGC isotherm at low loading. (c) Near critical adsorption in the 8σ pore: The GCE and CE isotherms are practically identical; the MDGC method is in excellent agreement with the IGGC method. (d) Subcritical capillary condensation in the 10σ pore: The CE isotherm has a sigmoid, van der Waals-type shape; the GCMC isotherm is reversible. The MDGC method is in excellent agreement with the IGGC method. The GCE isotherm reconstructed from the CE isotherm coincides with the GCMC isotherm.

In the supercritical region, the CE isotherms obtained with the IGGC method and GCE isotherm gradually merge, as the pore size increases, and become practically identical in the 8σ pore, where all three isotherms (IGGC, MDGC, and GCMC) collapse on the same curve. In the subcritical region, the CE isotherms differ significantly from the GCE isotherms in the two-phase region. The GCMC isotherm in the 10σ pore is reversible [Fig. 4(d)], while in the 15.8σ pore it is hysteretic with abrupt capillary condensation and desorption transitions (Fig. 5). The reversible GCMC isotherm can be reconstructed from the CE isotherm using Eq. (24) [Fig. 4(d)]. In larger pores (Fig. 5), GCMC isotherms are hysteretic, since the sampling is confined to the regions of vaporlike and liquidlike states, which are separated by insurmountable, at a given length of the simulation run, nucleation barriers.[32] In the hysteresis region, the vaporlike and liquidlike GCMC states match up with the CE states. The CE isotherm determined by the gauge cell method extends the GCMC isotherm in the region of metastable states to the very spinodals. The continuity of the CE isotherm allows one to determine the vapor–liquid equilibrium in the pore from the Maxwell rule of equal areas by the thermodynamic integration and to estimate the nucleation barriers for vapor–liquid and liquid–vapor transitions.[30,32] The backward trajec-

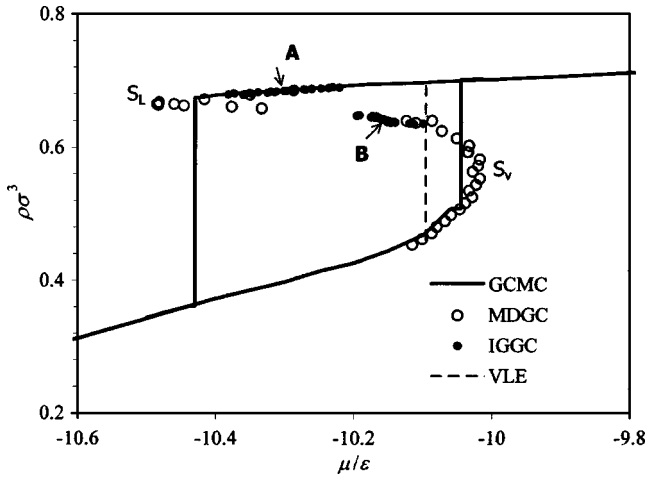

FIG. 5. Adsorption isotherms in the 15.8σ pore: The GCMC isotherm exhibits a hysteresis loop with abrupt capillary condensation and evaporation steps. The van der Waals-type CE isotherm produced with the MDGC method is continuous. It extends the GCMC isotherm in the regions of metastability up to the vaporlike and liquidlike spinodals (turnover points S_V and S_L). The backward trajectory corresponds to the states of critical nuclei unstable in GCE. Vapor–liquid equilibrium in the pore calculated via the Maxwell rule by thermodynamic integration along the CE isotherm is depicted by the broken vertical line. The closed circles present the states generated in IGGC simulations performed with the mean fluid densities, which correspond to liquidlike state A ($\bar{N}=1420$) and labile state B ($\bar{N}=990$).

tory of the CE isotherm corresponds to the states of critical nuclei, which would be unstable in the open system considered in GCE. A detailed analysis of the nucleation of liquid bridges and bubbles in the processes of condensation and evaporation is given elsewhere.[37,38]

It is worth noting that in the subcritical region the configurations of the confined fluid are highly inhomogeneous and the precision of the Widom method deteriorates rapidly as the pore widths increases. Already for the 10σ pore the use of the Widom method is impractical (see for details Figs. s3 and s4 in the Supplementary Information[47]).

VI. EXAMPLES OF MONTE CARLO SIMULATIONS: VARYING THE GAUGE CELL SIZE

The key property of the gauge cell method is the ability to control the density fluctuations in the system under study by varying the volume of the gauge cell. In this section, we show how the size of the gauge cell affects the fluctuations in the pore fluid and, vise versa, how the capacity of the pore affects the fluctuations in the gauge cell. Although the results of the gauge cell method do not depend on the gauge cell size, this issue is important for a rational choice of the size of the gauge cell for the most efficient simulations, especially in the case of relatively large systems containing 100 particles and more. As an example we focus on the simulations in the 15.8σ pore (Fig. 5).

Let us consider fluctuations of the number of particles in a sufficiently large system in MCE (as we will see below, "sufficiently large" means in practice that the total number of particles exceeds ~100 and the mean number of particles in the gauge cell exceeds ~10). In this case, the most probable distribution, $\hat{N}+\hat{N}_g=N_\Sigma$, is determined by Eq. (13) and the fluctuation around the most probable distribution is given by

$$P_{\hat{N}+n} = P_{\hat{N}} \exp\left\{-\frac{1}{kT}[F(\hat{N}+n)+F_g(\hat{N}_g-n)]\right\} \Big/ \exp\left\{-\frac{1}{kT}[F(\hat{N})+F_g(\hat{N}_g)]\right\}. \quad (26)$$

Developing the Helmholtz free energies in Eq. (26) into the Taylor series and leaving the second-order terms, we arrive at the Gaussian distribution of particles in MCE,

$$P_{\hat{N}+n} \approx P_{\hat{N}} \exp\left\{-\frac{n^2}{2\delta^2_{\mathrm{MCE}}}\right\}, \quad (27)$$

with the dispersion δ_{MCE} given by

$$\frac{1}{\delta^2_{\mathrm{MCE}}} = \frac{1}{kT\hat{N}^2\kappa/V} + \frac{1}{\hat{N}_g+1}. \quad (28)$$

Here, κ is the isothermal compressibility,

$$\kappa = \left(\frac{\hat{N}^2}{V}\left.\frac{\partial\mu}{\partial N}\right|_{V,T}\right)^{-1}, \quad (29)$$

and the second term in the right-hand side of Eq. (28) is the reciprocal mean-square deviation for the IG system at a given $\hat{N}_g$.

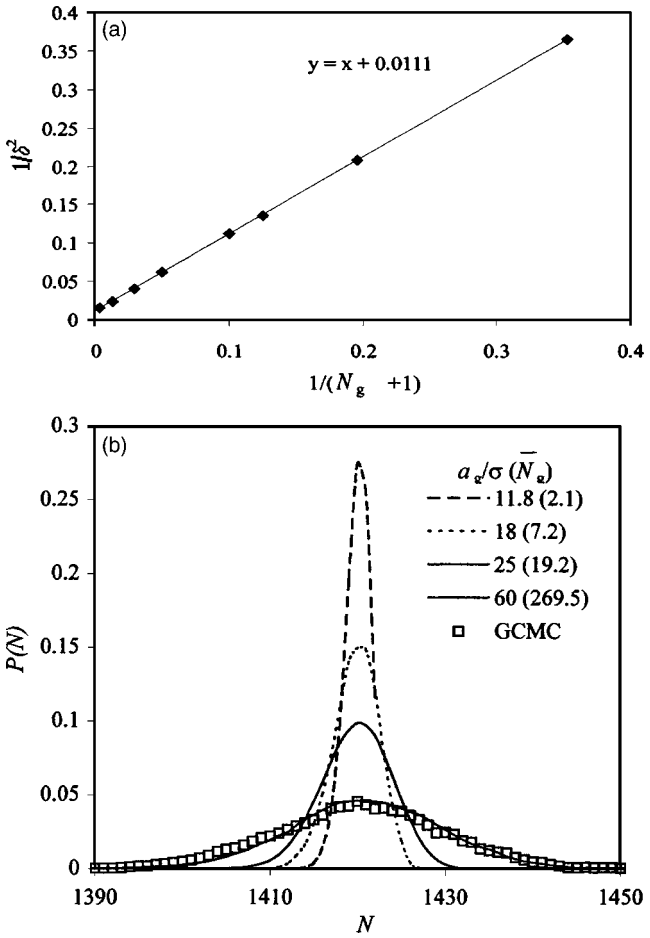

FIG. 6. Fluctuations of the number of molecules N in MCE sampled in the IGGC method in the 15.8σ pore at $\bar{N}=1420$. (a) Dependence of the dispersion of the particle distribution on the gauge cell mean capacity [Eq. (28)]. (b) Histograms of the number of particles in the pore cell sampled in IGGC simulations with gauge cells of different sizes. The legend shows the linear size of the cubic gauge cell a_g and the average number of molecules in the gauge cell in the course of simulation $\bar{N}_g$. As the gauge cell capacity increases the MCE distribution approaches the GCE distribution sampled in the GCMC simulation.

For the states, which are stable or metastable in the GCMC simulation, the isothermal compressibility [Eq. (29)] determines the dispersion of fluctuations in GCE,

$$\delta^2_{\mathrm{GCE}} = kT\hat{N}^2\kappa/V, \quad (30)$$

and Eq. (28) reduces to

$$\frac{1}{\delta^2_{\mathrm{MCE}}} \approx \frac{1}{\delta^2_{\mathrm{GCE}}} + \frac{1}{\hat{N}_g+1}. \quad (31)$$

Equation (31) determines the relation between the level of fluctuations in MCE and the size of the gauge cell. As the gauge size increases, MCE converges to GCE, and $\delta_{\mathrm{MCE}} \to \delta_{\mathrm{GCE}}$. The relation between the level of fluctuations and the size of the gauge cell is illustrated in Figs. 6(a) and 6(b) which show the fluctuations of N and N_g in the simulations of liquidlike states with the mean number of molecules in the pore, $\bar{N}=1420$ (point A in Fig. 5). The states sampled in IGGC simulations are shown as a series of very closely spaced points around A. The gauge cell volume V_g was var-

ied from $(11.2\sigma)^3$ to $(60\sigma)^3$ and the total number of molecules N_Σ was adjusted, respectively, to keep the mean number of molecules in the pore constant $\overline{N}=1420$. The constraints gradually "loosen up" as V_g increases, with $1/\delta^2$ increasing linearly with $\overline{N_g}+1$ as predicted by Eq. (24), which holds almost exactly [Fig. 6(a)]. At $V_g=(60\sigma)^3$ the distribution approaches the distribution sampled in the GCMC simulation at the corresponding chemical potential $\mu=\mu_{\mathrm{CE}}(\overline{N})$ [Fig. 6(b)]. A single IGGC simulation produces an interval of points on the isotherm (Fig. 5). The larger the gauge, the wider the interval sampled in the simulation and the higher the statistical uncertainty of each point, which increases quickly to the periphery of the histogram. The complete discrete isotherm $N(\mu)$ (similar to those presented in Figs. 2 and 4) may be obtained via a series of simulations with different $\overline{N}$ ranging from zero to a dense liquid provided that the distributions in the neighboring simulations are overlapping. If the system is large enough, the complete discrete isotherm is not required, since the isotherm may be interpolated easily between fewer points. In doing so, the compressibility, which may also be determined from IGGC simulations, should not vary substantially between the neighboring points. In this case, the MDGC method works well and can be used instead of the IGGC method, which is more time consuming. As seen from Figs. 4 and 5, starting from the 8σ pore, a reasonable interpolation does not compromise the quality of the isotherm.

One of the main advantages of the gauge cell method is the ability to construct the metastable states near the spinodals and the labile states on backward trajectory of the CE isotherm, which cannot be sampled in GCE simulation (Fig. 5). A series of states sampled in a single IGGC simulation is shown as very closely spaced points around the most probable state B. The level of fluctuations sampled in MCE simulation for the states on the backward trajectory of the CE isotherm, which have a "negative" compressibility $\kappa=((N^2/V)\,(\partial\mu/\partial N)|_{V,T})^{-1}<0$, is determined by Eq. (28), in which one term is negative and the other is positive. Being unstable in GCE, these labile states are "stabilizable" in MCE provided that the gauge cell size is sufficiently small so that the positive contribution from the gauge cell overweighs the negative contribution from the pore fluid. The condition of stabilization of labile states reads as

$$\frac{1}{\delta^2_{\mathrm{MCE}}}=\frac{1}{kT\hat{N}^2\kappa/V}+\frac{1}{\hat{N}_g+1}>0. \tag{32}$$

Thus, in order to generate labile states in the gauge cell MC method, the ratio of the volumes of the gauge cell and the pore cell should fulfill the inequality[30]

$$\frac{V_g}{V}<\frac{kT|\kappa|\rho^2}{\rho_g}, \tag{33}$$

where ρ and ρ_g are, respectively, the density of the labile state $[N(\mu)/V]$ and the ideal-gas density at a given μ. The computations of labile states and metastable liquidlike states are similar. For a "large" system presented in Fig. 5, the MDGC method is applicable and it is more practical than the IGGC method except for the regions near the spinodals. However, as the compressibility decreases, the gauge size required to stabilize the system decreases, which affects the precision of the chemical-potential calculation as shown in the next paragraph. In the vicinity of superspinodals, where $|\kappa|\to 0$ (Refs. 42 and 53) the gauge cell method cannot be applied.

Fluctuations in the pore cell are coupled with fluctuations in the gauge cell [Eq. (31)]. When the system is so large that $\delta_{\mathrm{GCE}}\gg\hat{N}_g^{1/2}$, the pore cell plays the role of an unlimited reservoir of particles for the gauge cell. That is, the probability distribution in the gauge cell, $P(N_g)$, can be compared with the probability distribution of the ideal gas in GCE,

$$\frac{P(N_g+1)}{P(N_g)}=\frac{V_g}{\Lambda^3(N+1)}\exp\left(\frac{\mu_{\mathrm{id}}}{kT}\right), \tag{34}$$

with the chemical potential μ_{id} being an adjustable parameter. This correlation is demonstrated in Fig. 7. With a small gauge that typically has several molecules in the course of simulation, the probability distribution curve is highly asymmetric [Fig. 7(a)]. As a result, the chemical potential calculated from the mean density in the gauge cell using Eq. (16) exceeds the actual value [of about 0.06ε in the case shown in Fig. 7(a)], and the difference cannot be reduced by increasing the simulation length. The difference of 0.06ε is quite notable in many practical applications, including pore size characterization from adsorption isotherms.[48] Thus, in order to efficiently apply the MDGC method, the gauge cell has to be large enough to provide a symmetric distribution of the number of particles around the most probable. In the example shown in the figure, a practically ideal symmetric distribution is achieved at about $V_g=(18\sigma)^3$ which corresponds to $\overline{N_g}\approx 7$ [Fig. 7(b)], and MDGC perfectly agrees with IGGC. That is, seven molecules is an optimal gauge cell capacity in this particular case. As the gauge cell size increases further, the contribution from the pore cell into Eq. (31) becomes appreciable, and the particle distribution in the gauge cell cannot be fitted by that of the ideal gas [Fig. 7(d)]. Yet, $P(N_g)$ remains symmetric and quasi-Gaussian, so that Eq. (16) gives excellent agreement with Eq. (15). Thus, as long as the variation of the pore fluid compressibility $\kappa=((N^2/V)\,(\partial\mu/\partial N)|_{V,T})^{-1}$ is negligible within the interval of N sampled in the simulation, the MDGC method based on Eq. (16) works for relatively large systems as those considered in Refs. 30, 32, 34, 36, and 37.

VII. CONCLUSION

We have presented the ideal-gas gauge cell (IGGC) method for the calculation of the chemical potential in small inhomogeneous systems. The IGGC method is based on the mesoscopic canonical ensemble (MCE) computation scheme. It allows one to determine in a single simulation the chemical potentials of a series of states differing by one molecule and to construct the canonical ensemble isotherm, which contains the detailed information about the system. The statistical mechanical framework of the method was presented. The specifics and advantages of the method were

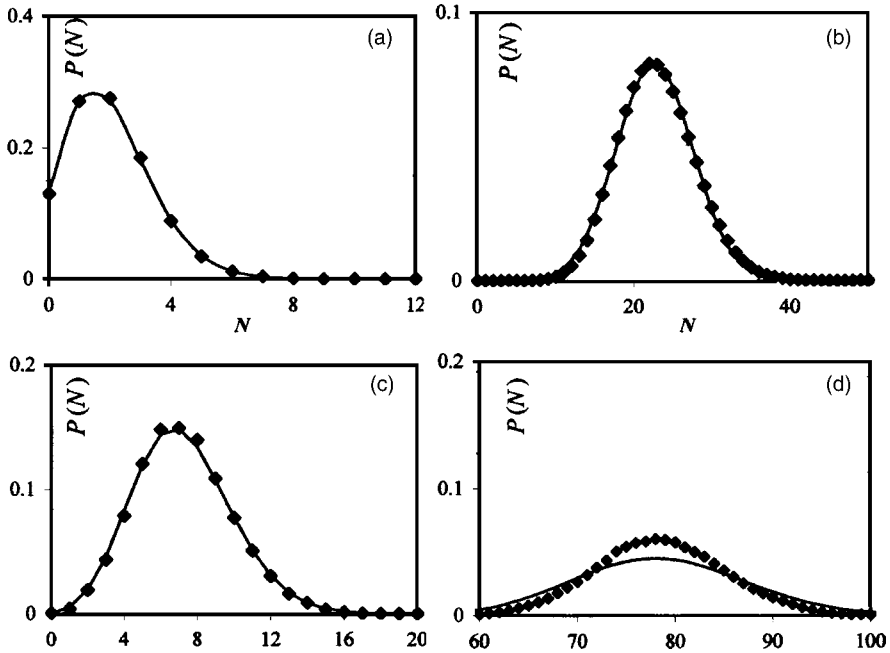

FIG. 7. Histograms of the number of particles in the gauge cells of different sizes in the 15.8σ pore at $kT/\varepsilon=0.762$. $V_g=$(a) $(12\sigma)^3$, (b) $(18\sigma)^3$, (c) $(30\sigma)^3$, and (d) $(40\sigma)^3$ fitted by GCE distributions of ideal particles [Eq. (34)]. The average number of molecules in the pore cell is $\bar{N}=1420$ (point A in Fig. 5). GCE distributions are held in sufficiently small gauge cells.

demonstrated on studies of the phase equilibrium in a Lennard-Jones fluid confined to spherical pores of different diameters. Special attention was paid to the conditions of extreme confinement where the results of the canonical and grand canonical ensembles deviate substantially and the Widom method is not practical. In the systems, which contain a sufficiently large amount of particles ($>\sim 60$ at these conditions), the IGGC method can be substituted with the mean density gauge cell (MDGC) method proposed earlier.[30] We have analyzed the effect of the gauge cell size on the efficacy of simulations and demonstrated that the gauge cell, which accommodates on average >8 particles, is satisfactory for reliable MDGC calculations. Being as computationally efficient as the GCMC method, the gauge cell method can be considered as a practical alternative to the Widom method for the calculation of the chemical potential in small, dense, inhomogeneous systems, including metastable states and labile states, which are stable in the canonical ensemble and unstable in the grand canonical ensemble. This opens up an opportunity to study metastable equilibrium and hysteretic phase transitions observed in small confined systems. The transition from supercritical adsorption to subcritical capillary condensation, which is observed as the pore size increases, was illustrated with the model system mimicking nitrogen sorption at the normal boiling temperature in silica pores ranging from 4 to 15.8 molecular diameters.

The computer programs for the IGGC and MDGC MC simulations are provided in the Supplementary Information.[47]

ACKNOWLEDGMENTS

The work was supported by the TRI/Princeton exploratory research program. One of the authors (A.V.N.) gratefully acknowledges the support of the John Simon Guggenheim Memorial Foundation and fruitful discussions with J. K. Percus and Ya. G. Sinai.

[1] B. Widom, J. Chem. Phys. **39**, 2808 (1963).
[2] D. Frenkel and B. Smit, *Understanding Molecular Simulation. From Algorithms to Applications* (Academic, San Diego, 1996).
[3] D. P. Landau and K. Binder, *A Guide to Monte Carlo Simulations in Statistical Physics* (Cambridge University Press, Cambridge, 2000).
[4] N. Metropolis, A. W. Rosenbluth, M. N. Rosenbluth, A. H. Teller, and E. Teller, J. Chem. Phys. **21**, 1087 (1953).
[5] K. S. Shing and K. E. Gubbins, Mol. Phys. **43**, 717 (1981).
[6] C. H. Bennett, J. Comput. Phys. **22**, 245 (1976).
[7] G. C. Boulougouris, I. G. Economou, and D. N. Theodorou, J. Chem. Phys. **115**, 8231 (2001).
[8] G. C. Boulougouris, I. G. Economou, and D. N. Theodorou, Mol. Phys. **96**, 905 (1999).
[9] W. C. Swope and H. C. Andersen, J. Chem. Phys. **102**, 2851 (1995).
[10] D. Frenkel and B. Smit, Mol. Mater. **75**, 983 (1992).
[11] G. Mooij, D. Frenkel, and B. Smit, J. Phys.: Condens. Matter **4**, L255 (1992).
[12] S. Consta, T. J. H. Vlugt, J. W. Hoeth, B. Smit, and D. Frenkel, Mol. Phys. **97**, 1243 (1999).
[13] S. Consta, N. B. Wilding, D. Frenkel, and Z. Alexandrowicz, J. Chem. Phys. **110**, 3220 (1999).
[14] J. R. Henderson, Mol. Phys. **90**, 581 (1997).
[15] N. G. Parsonage, Mol. Phys. **89**, 1133 (1996).
[16] I. Nezbeda and J. Kolafa, Mol. Simul. **5**, 391 (1991).
[17] A. P. Lyubartsev, A. A. Martsinovski, S. V. Shevkunov, and P. N. Vorontsov-Velyaminov, J. Chem. Phys. **96**, 1776 (1992).
[18] P. Attard, J. Chem. Phys. **98**, 2225 (1993).
[19] J. P. Valleau and D. N. Card, J. Chem. Phys. **57**, 5457 (1972).
[20] K. J. Ding and J. P. Valleau, J. Chem. Phys. **98**, 3306 (1993).
[21] D. A. Kofke and P. T. Cummings, Mol. Phys. **92**, 973 (1997).
[22] M. Athenes, Phys. Rev. E **66**, 046705 (2002).
[23] G. Domotor and R. Hentschke, J. Phys. Chem. B **108**, 2413 (2004).
[24] D. S. Corti and M. Heying, Fluid Phase Equilib. **204**, 183 (2003).
[25] B. Widom, J. Stat. Phys. **19**, 563 (1978).
[26] J. G. Powles, S. E. Baker, and W. A. B. Evans, J. Chem. Phys. **101**, 4098 (1994).
[27] J. G. Powles, B. Holtz, and W. A. B. Evans, J. Chem. Phys. **101**, 7804 (1994).

[28] J. F. Knight and P. A. Monson, Mol. Phys. **60**, 921 (1987).
[29] S. Tripathi and W. G. Chapman, Mol. Phys. **101**, 1199 (2003).
[30] A. V. Neimark and A. Vishnyakov, Phys. Rev. E **62**, 4611 (2000).
[31] M. Jorge and N. A. Seaton, Mol. Mater. **100**, 3803 (2002).
[32] A. Vishnyakov and A. V. Neimark, J. Phys. Chem. B **105**, 7009 (2001).
[33] A. Vishnyakov and A. V. Neimark, Langmuir **19**, 3240 (2003).
[34] M. Jorge and N. A. Seaton, Stud. Surf. Sci. Catal., **144**, 131 (2002).
[35] M. Jorge, C. Schumacher, and N. A. Seaton, Langmuir **18**, 9296 (2002).
[36] J. W. Jiang, S. I. Sandler, and B. Smit, Nano Lett. **4**, 241 (2004).
[37] A. Vishnyakov and A. V. Neimark, J. Chem. Phys. **119**, 9755 (2003).
[38] A. V. Neimark and A. Vishnyakov, J. Chem. Phys. **122**, 054707 (2005).
[39] A. V. Neimark and A. Vishnyakov, J. Chem. Phys. **122**, 174508 (2005).
[40] G. E. Norman and V. S. Filinov, High Temp. **7**, 216 (1969).
[41] B. K. Peterson and K. E. Gubbins, Mol. Phys. **62**, 215 (1987).
[42] A. V. Neimark, P. I. Ravikovitch, and A. Vishnyakov, Phys. Rev. E **65**, 031505 (2002).
[43] A. Z. Panagiotopoulos, Mol. Phys. **62**, 701 (1987).
[44] A. Z. Panagiotopoulos, Mol. Phys. **61**, 813 (1987).
[45] A. Gonzalez, J. A. White, F. L. Roman, and R. Evans, J. Chem. Phys. **109**, 3637 (1998).
[46] J. K. Johnson, J. A. Zollweg, and K. E. Gubbins, Mol. Phys. **78**, 591 (1993).
[47] See EPAPS Document No. E-JCPSA6-123-512526 for the supplementary figures, the program for the GCMC/CEMC/IGGC/MDGC simulations that was applied in this paper, and the manual to the program. Supplementary Fig. s1 shows the CE and GCE isotherms in the 4σ pore at $kT/\varepsilon=0.6$, 0.762, and 0.85. Figures s2 and s3 show the comparison of the GCMC, MDGC, and Widom particle insertion method simulations in 10σ and 15.8σ pores at $kT/\varepsilon=0.762$. The program (Fortran source code given) is designed for the simulations of rigid molecules of any shape in bulk or pores (slit, cylindrical, or spherical) with pretabulated solid–fluid potential. A program for the calculation of the potential in spherical pores formed by LJ particles is also included. This document can be reached via a direct link in the online article's HTML reference section or via the EPAPS homepage (http://www.aip.org/pubservs/epaps.html).
[48] P. I. Ravikovitch, A. Vishnyakov, R. Russo, and A. V. Neimark, Langmuir **16**, 2311 (2000).
[49] P. I. Ravikovitch and A. V. Neimark, Langmuir **18**, 1550 (2002).
[50] P. I. Ravikovitch, S. C. Odomhnaill, A. V. Neimark, F. Schuth, and K. K. Unger, Langmuir **11**, 4765 (1995).
[51] J. H. deBoer, B. G. Linsen, and T. J. Osinga, J. Catal. **4**, 643 (1965).
[52] W. A. Steele, *The Interactions of Gases with Solid Surfaces* (Pergamon, New York, 1974).
[53] A. V. Neimark and A. Vishnyakov, J. Phys. Chem. B **109**, 5962 (2005).